

# SYNTHESIS AND CHARACTERIZATION OF BIOACTIVE GLASS/FORSTERITE NANOCOMPOSITES FOR BONE AND DENTAL IMPLANTS

REZA KAMALIAN, ABOLFAZL YAZDANPANAHI, FATHOLLAH MOZTARZADEH, ROYA RAVARIAN\*, ZOHA MOZTARZADEH\*\*, MOHAMMAD TAHMASBI\*\*\*, #MASOUD MOZAFARI\*, \*\*\*\*

*Biomaterials Group, Faculty of Biomedical Engineering (Center of Excellence), Amirkabir University of Technology, P. O. Box: 15875-4413, Tehran, Iran*

*\* School of Chemical and Biomolecular Engineering, The University of Sydney, New South Wales, NSW 2006, Australia*

*\*\* Institute of Bioinformatic, Münster University, Münster, Germany*

*\*\*\* School of Mechanical Engineering, Sharif University of Technology, Tehran, Iran*

*\*\*\*\* Helmerich Advanced Technology Research Center, School of Material Science and Engineering, Oklahoma State University, OK 74106, USA*

#E-mail: masoud.mozafari@okstate.edu

Submitted December 8, 2011; accepted October 26, 2012

**Keywords:** Nanocomposite, Bioactive CaO–P<sub>2</sub>O<sub>5</sub>–SiO<sub>2</sub> glass, Forsterite bioceramic, Sol-gel method, Bone implant

*In this research, bioactive glass (BG) of the type CaO–P<sub>2</sub>O<sub>5</sub>–SiO<sub>2</sub> and nanocrystalline forsterite (NF) bioceramic were successfully synthesized via sol–gel processing method. Heat-treatment process was done to obtain phase-pure nanopowders. After characterization of each sample, the nanocomposite samples were prepared by cold pressing method and sintered at 1000°C. The samples were fully characterized by X-ray powder diffraction (XRD), scanning electron microscope (SEM), energy dispersive spectroscopy (EDX), Fourier transform infrared spectroscopy (FTIR) analyses. The average nanocrystallite size was determined using the Debye-Scherrer's formula 19.6 nm. The bioactivity was examined in vitro with respect to the ability of hydroxyapatite (HAp) layer to form on the surfaces as a result of contact with simulated body fluid (SBF). According to the obtained results, the prepared nanocomposite enhances the fracture toughness of the BG matrix without deteriorating its intrinsic properties as bioactivity.*

## INTRODUCTION

During the past years, different concepts for microstructure design have been proposed to overcome the inherent brittleness of ceramics [1-3] but the predicted improvements have not been achieved. In the range of ceramic materials, and according to their nanostructure, bioactive glasses (amorphous solid materials) are placed at the farthest end from the conventional ceramics (crystalline solid materials) [4]. Bioactive glasses are defined by Hench [5, 6] as materials capable to create a chemical bond with surrounding tissues without interposition of a fibrous layer. These materials exhibit osteoconductive properties, defined as the characteristic of bone growth in porosities and bonding along the surface.

When in contact with body fluids or tissues, BGs develop reactive layers at their surfaces resulting in a chemical bond between implant and host tissue [7]. Hench et al. [8] have described a sequence of five reactions that result in the formation of a hydroxy-carbonate apatite (HCA) layer on the surface of BGs [9]. The characteris-

tic amorphous quality of BGs is their open structure arrangement which facilitates the inclusion of cations referred as network modifiers, causing a discontinuity of the glassy network and consequently, non-bridging oxygen is released [10-13]. This high reactivity is the main advantage of their application in periodontal repair and bone augmentation [14]. This is due to the reaction [15] products obtained from these types of glasses and physiological fluids resulting in crystallized apatite-like phase similar to the inorganic component of bones in vertebrate species [16, 17]. BGs have the advantage of being close to the composition of natural bone, but their disadvantage lies in their low mechanical strength which limits their applications. Toughness is often an important property required for BGs and glass-ceramics. Also, for long-term implants, it may be important to increase the toughness as much as possible without losing bioactivity.

In recent years, some Si and Mg containing ceramics have drawn interests in the development of bone implant materials [18-21]. Nanocrystalline forsterite (NF) is an important material in the magnesia–silica system [22]. Compared with hydroxyapatite ceramics, NF ceramics

showed a significant improvement in the fracture toughness about  $2.4 \text{ MPa}\cdot\text{m}^{1/2}$  which superior to the lower limit reported for bone implant [23]. *In vitro* studies showed significant osteoblast adhesion, spreading and growth on the surface of NF ceramic [23]. Ni et al. [23, 24] showed that NF ceramic is a novel bioceramic with high mechanical properties and good biocompatibility and might be suitable for hard tissue repair. However, the degradation rate of NF ceramic is extremely low, and the apatite-formation ability is also poor [24]. In addition, NF is a crystalline magnesium silicate with the chemical formula  $\text{Mg}_2\text{SiO}_4$ , named after the German scientist Johann Forster [25-27].

Improvement of mechanical features of ceramic based bone implants is important for the osteointegration process. It is known that nanostructured ceramics have superior mechanical properties [28]. In addition, the nanometersized grains and the high volume fraction of grain boundaries in nanostructured materials are reported to show improved biocompatibility over normal materials [29-32], and increased the activity of osteoblast cells [33]. After designing the first nanophase ceramics with the aim of improving osteointegrative properties of orthopedic and dental materials, researchers found out that in contrast to conventional materials, nanophase ceramics can be designed with surface properties, mechanical properties, and grain size distribution similar to natural bone [34].

According to the above points, nanostructured NF bioceramic is expected to have even better mechanical properties and biocompatibility than coarser crystals. It was reported that coarse grain NF had an extremely low degradation rate and was not bioactive. Recent studies in this field indicated that NF nanopowder, unlike micron-sized forsterite, possessed apatiteformation ability. The bioactivity of the NF when compared to coarse grain forsterite shows a greater effect of the nanophase forsterite on its ion dissolution in biological solution [35]. According to the previous explanations, the addition of NF can improve the mechanical properties of the implants needed for bone defect repairing. In this research, the nanocomposites were prepared from nanopowder with different NF additions to study their effect on the surface bioactivity and mechanical properties of the BG-based nanocomposites.

## EXPERIMENTAL

### Materials

Tetraethylorthosilicate TEOS ( $\text{C}_2\text{H}_5\text{O}$ )<sub>4</sub>Si, calcium nitrate ( $\text{Ca}(\text{NO}_3)_2\cdot 4\text{H}_2\text{O}$ ), triethyl phosphate TEP ( $\text{C}_2\text{H}_5$ )<sub>3</sub>PO<sub>4</sub> and 0.1 M nitric acid ( $\text{HNO}_3$ ) were purchased from Merck Inc. to synthesize the BG powder. Also, magnesium nitrate ( $\text{Mg}(\text{NO}_3)_2\cdot 6\text{H}_2\text{O}$ ), sucrose as a template material, PVA (polyvinyl alcohol,  $M_w = 145,000$ ), nitric acid (all purchased from Merck, Germany) and colloidal

silica with particle size smaller than 14 nm (26 wt. % solid fraction-from Monatso Co., Belgium) were used as starting materials to synthesis the NF particles.

### Preparation of BG nanoparticles

The sol-gel derived BG consisting of 64 % SiO<sub>2</sub>, 5 % P<sub>2</sub>O<sub>5</sub>, and 31 % CaO (mol. %) was synthesized as follows: 14.8 g (0.064 mol) of TEOS was added into 30 ml of 0.1 M nitric acid, the mixture was allowed to react for 30 min for the acid hydrolysis of TEOS to proceed almost to completion. The following reagents were added in sequence allowing 45 min for each reagent to react completely: 0.85 g (0.005 mol) TEP, and 7.75 g (0.031 mol) of calcium nitrate tetrahydrate. After the final addition, mixing was continued for 1 h to allow completion of the hydrolysis reaction. The solution was cast in a cylindrical Teflon container and kept sealed for 10 days at room temperature to allow the hydrolysis and a polycondensation reaction to take place until the gel was formed. The gel was kept in a sealed container and heated at 70°C for an additional 3 days. The water was removed and a small hole was inserted in the lid to allow the leakage of gases while heating the gel to 120°C for 2 days to remove all the water. Subsequently, the powder was milled for 10 h by planetary mill (SVD15IG5-1, LG Company).

### Preparation of NF

In this research, NF was synthesized as follows: Briefly, a transparent sol was prepared by dissolving 0.0142 mol magnesium nitrate in 50 ml of de-ionized water. Next, 0.0071 mol of silica (1.642 g of colloidal silica) was introduced into the solution to set MgO/SiO<sub>2</sub> molar ratio to 2:1 which corresponds to the theoretical value of pure NF. As the second solution which was prepared separately, 0.0568 mol sucrose was added into 100 ml of de-ionized water. Then, two solutions were mixed together and continuously stirred for 2 h. In the next step, 0.0071 mol of PVA was mixed with 20 ml of de-ionized water to prepare a PVA solution and then was added into the final solution and pH was adjusted to 1 by drop-wise addition an appropriate amount of diluted nitric acid, and finally the mixture stirred for 4 h. Here, the mole ratio of the Mg<sup>2+</sup> ions, sucrose and PVA monomer was 1:4:0.5. According to Tsai *et al.* [36], the addition of nitrate acid causes the breaking of sucrose into glucose and fructose which prevents the recrystallization of sucrose molecular structure. The -OH and -COOH groups of decomposed products promote binding of Mg<sup>2+</sup> ions in homogeneous solution. With the aim of letting the Mg<sup>2+</sup> ions react with sucrose completely the solution heated at 80°C for 2 h on a hot plate stirrer, and then heated in an electric oven at 200°C for complete dehydration and changing into a viscous dark brownish gel. The prepared gel trapped nanoparticles of colloidal

silica. During additional heating, the obtained gel in the oven converted to black foamed mass. Subsequently, the obtained mass was milled into fine powder by planetary milling (SVD15IG5-1, LG Company) with 400 rpm during 2 h. After grinding and sieving, the dry powder calcined for 3 h at 900°C. According to Saberi *et al* [37], the calcinations process decomposed polymeric matrix into gases such as CO<sub>2</sub> and H<sub>2</sub>O and resulting in a large amount of released heat. These produced gases prevent from agglomeration of calcined powders. During the calcination, existed carbon in the black precursor powder was burned out and a white color powder was formed.

### Specimen preparation

The synthesized BG powder was mixed with different ratios (wt. %) of the synthesized NF to prepare BG/NF nanocomposite samples (NC0:100/0, NC1:90/10, NC2:80/20, NC3:70/30). The mixtures were prepared in a planetary ball mill (Retch PMA, Brinkman, USA) for 30 min to ensure homogeneity. Each batch was carefully mixed with 0.1 wt. % of carboxymethyl cellulose (CMC) as the binding agent. Then, the mixtures were formed to disks using cold press molding method. Green compact disks were achieved by using a predetermined amount of mixed powder, which resulted in the targeted thickness (about 15 mm) after being pressed uniaxially in a steel die of 13 mm in diameter under the pressure of 50 MPa. Finally, composites were sintered at 1000°C for 2 h.

### Preparation of SBF solution

The SBF solution was prepared by dissolving reagent-grade NaCl, KCl, NaHCO<sub>3</sub>, MgCl<sub>2</sub>·6H<sub>2</sub>O, CaCl<sub>2</sub> and KH<sub>2</sub>PO<sub>4</sub> into distilled water and buffered at pH = 7.25 with TRIS (trishydroxymethyl aminomethane) and 1N HCl solution at 37°C. Its composition is given in Table 1 and is compared with the human blood plasma. It should be also noted that SBF is a solution highly supersaturated with respect to apatite [38]. For these dense materials, we measured the sample dimensions and calculated the surface area with an accuracy of 2 mm<sup>2</sup> for the thin plates. We calculated the volume of SBF that was used for testing using the following Equation 1:

$$V_s = S_a/10 \quad (1)$$

where  $V_s$  is the volume of SBF (ml) and  $S_a$  is the apparent surface area of specimen (mm<sup>2</sup>). For The calculated volume of SBF into was put in plastic bottles. After heating the SBF to 36.5°C the samples were placed in the SBF. After soaking at 36.5°C in the SBF, the samples were taken out from the SBF and were gently washed with pure water, and then were dried in a desiccator without heating. The samples once taken out of SBF and dried and have not been soaked again.

Table 1. Ion concentrations of simulated body fluid (SBF) and human blood plasma.

Ion	Plasma (mmol/l)	SBF (mmol/l)
Na <sup>+</sup>	142.0	142.0
K <sup>+</sup>	5.0	5.0
Mg <sup>+2</sup>	1.5	1.5
Ca <sup>+2</sup>	2.5	2.5
Cl <sup>-</sup>	103.0	147.8
HCO <sub>3</sub> <sup>-</sup>	27.0	4.2
HPO <sub>4</sub> <sup>-2</sup>	1.0	1.0
SO <sub>4</sub> <sup>-2</sup>	0.5	0.5

### Sample characterization

#### XRD analysis

The samples surfaces were analyzed by XRD with Siemens-Brucker D5000 diffractometer. This instrument works with voltage and current settings of 40 kV and 40 mA respectively and uses Cu-K $\alpha$  radiation (1.540600 Å). For qualitative analysis, XRD diagrams were recorded in the interval 10° ≤ 2θ ≤ 50° at scan speed of 2°/min.

#### SEM analysis

The morphology and microstructure of the synthesized nanocomposite samples were evaluated using SEM. The samples were coated with a thin layer of Gold (Au) by sputtering (EMITECH K450X, England) and then the morphology of them were observed on a scanning electron microscope (SEM-Philips XL30) that operated at the acceleration voltage of 15 kV.

#### EDX analysis

Energy dispersive X-ray analyzer (EDX, Rontec, Germany) connected to SEM was used to investigate semi-quantitatively chemical compositions.

#### FTIR analysis

The samples were examined by FTIR with Bomem MB 100 spectrometer. For IR analysis, 1 mg of the scraped samples were carefully mixed with 300 mg of KBr (infrared grade) and palletized under vacuum. Then, the pellets were analyzed in the range of 500 - 4000 cm<sup>-1</sup> with 4 cm<sup>-1</sup> resolution averaging 120 scans.

#### Mechanical behavior

Mechanical behavior of the prepared nanocomposite samples was investigated by using compression strength test. The cylindrical specimens were prepared to an appropriate size (13 mm in diameter and 15 mm in

thickness), and the thicknesses were measured with an electric digital caliper. Then, the compressive strengths of the wet samples were measured by a Zwick/Roell Universal Testing Machine apparatus with a crosshead speed of 1 mm/min. The following equations were used for the calculation of  $E$  (elastic constant) (2) [39, 40] and  $\sigma$  (yield stress) (3):

$$E = KL/A \quad (2)$$

$$\sigma = F/A \quad (3)$$

where  $F$  is ultimate load;  $K$  is stiffness;  $L$  is length of sample;  $A$  is average of surface area calculated from the following equation (4):

$$A = \pi/2 \times 1/4(d_1^2 + d_2^2) \quad (4)$$

where  $d_1$  and  $d_2$  are the diameters of the bases of the cylindrical samples. The fracture toughness of the samples was obtained from the area under the stress-strain curve normalized by the specimen's surface area. Each test has been repeated five times and the average amount and standard deviation (SD) of related parameters was determined.

#### *In vitro* bioactivity study in SBF solution

We carried out *in vitro* studies by soaking the nanocomposite samples in SBF solution at 37°C for 14 days. At regular intervals (1, 3, 7, 14 days) samples were taken out and rinsed with doubly distilled water, and dried in an oven at 40°C for 10 h before analysis by SEM and EDX.

#### Statistical analysis

All experiments were performed in fifth replicate. The results were given as means  $\pm$  standard error (SE). Statistical analysis was performed by using One-way ANOVA and Tukey test with significance reported when  $P < 0.05$ . Also for investigation of group normalizing, Kolmogorov-Smirnov test was used.

## RESULTS AND DISCUSSION

### XRD pattern of the synthesized NF powder

The phase purity and phase structure of the NF sample were carried out by XRD analysis as shown in Figure 1a. The XRD patterns showed the formation of single-phase pure NF obtained by heat-treatment at 900°C. As it can be seen for the NF sample, the significant and sharp diffraction peaks suggested that the obtained nanopowder was highly crystalline. According to the JCPDS data file No. 34-0189, all the characteristic peaks of NF phase were obviously detected. The XRD analysis also showed some small peaks which may be related to

the formation of a small amount of enstatite (according to JCPDS data file No. 11-0273) [41] along with NF at higher temperatures. The average nanocrystallite size was determined from the half-width of main diffraction peaks using the Debye-Scherrer's formula (1):

$$D = k\lambda/\beta \cos \theta \quad (1)$$

where  $D$  is the crystallite diameter,  $k$  is a constant (shape factor, about 0.9),  $\lambda$  is the X-ray wavelength (1.5405 Å),  $\beta$  is the full width at half maximum (FWHM) of the diffraction line, and  $\theta$  is the diffraction angle. The average crystallite size was estimated approximately 19.5 nm.

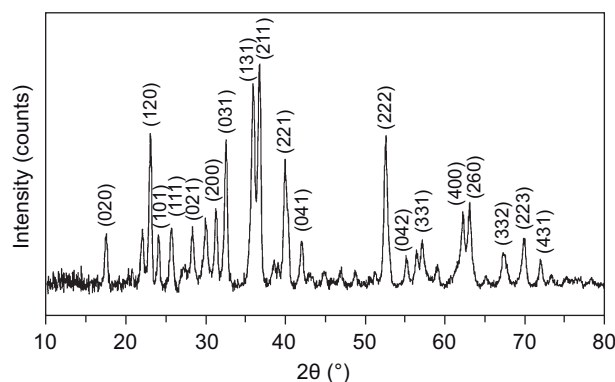


Figure 1. XRD pattern of the synthesized NF nanoparticles.

### SEM-EDX analyses of the synthesized NF

The low and high magnification SEM micrographs of the synthesized nanocrystalline forsterite are shown in Figure 2a. As it can be seen in these figures, heterogeneous surfaces consisting of random-sized particles with sharp edges and voids among them are shown. In addition, some agglomerated particles are probably seen that can be separated easily due to the nanocrystalline nature of the synthesized sample. Furthermore, Figure 2b shows the EDX spectra of the synthesized single-phase nanocrystalline forsterite. The EDX spectrum shows the peaks of Mg, Si, and O which are the main components of the prepared sample. The presence of gold (Au) on the BG surfaces was only related to the sputtering before SEM analysis. According to the obtained results, it is worth mentioning that the EDX analysis revealed that the compositions of the sample were Mg, Si and O closely similar to that of bulk  $Mg_2SiO_4$  (Mg:Si:O=2:1:4) [42-44].

### FTIR analysis

Figure 3 shows the FTIR spectra, in the 500 - 4000  $cm^{-1}$  spectral range, of the synthesized NC1, NC2 and NC3 nanocomposite samples to determine the chemical bonds and compositions. It is worth to note that the FTIR spectra of the nanocomposite samples exhibited

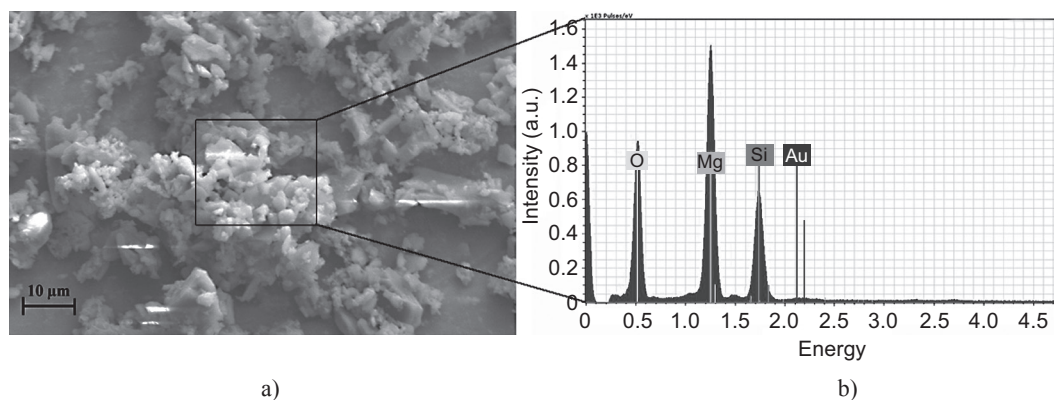


Figure 2. SEM micrograph (a) and EDX pattern (b) of the synthesized NF nanoparticles.

a number of characteristic spectral bands related to BG and NF particles. According to this figure, all the FTIR spectra exhibited some infrared bands related to the BG phase located at: 609, 800, 930, 1070 and 1212  $\text{cm}^{-1}$ . Among these bands, those positioned at 800, 930, 1070 and 1212  $\text{cm}^{-1}$  are related to the silicate network and respectively ascribed to the Si–O symmetric stretching of bridging oxygen atoms between tetrahedrons, Si–O stretching of non-bridging oxygen atoms, Si–O–Si symmetric stretching, and the LO mode (out-of-phase motion of adjacent oxygen atoms) of Si–O–Si asymmetric stretching. The band located at 609  $\text{cm}^{-1}$  is attributed to the asymmetric vibration of  $\text{PO}_4^{3-}$  [45-49].

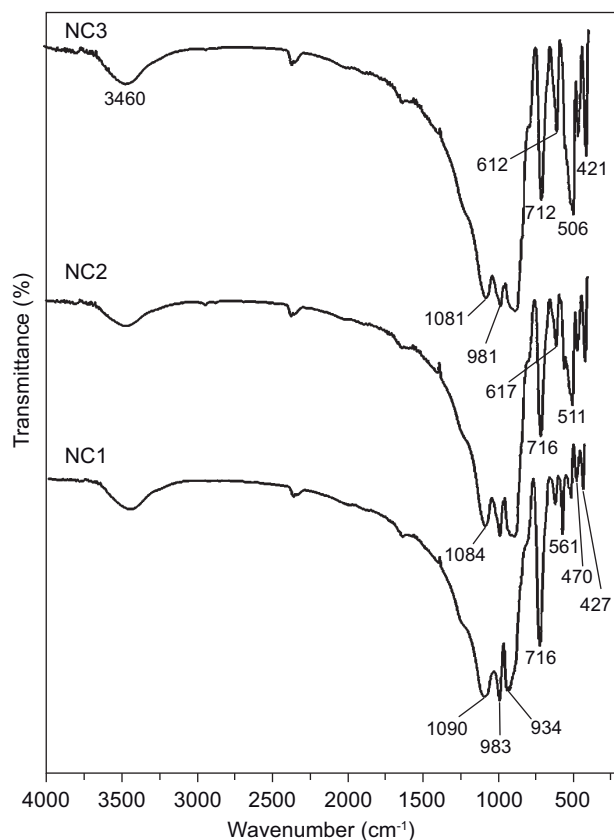


Figure 3. The FTIR spectra of the BG/NF nanocomposite samples with different percentages of BG and NF.

In addition, the main characteristic bands of ideal NF can be seen in this figure. For instance, the bands related to the characteristic peaks of NF appeared at 488 and 643  $\text{cm}^{-1}$  for  $\text{SiO}_4$  bending, at 910 and 1092  $\text{cm}^{-1}$  for  $\text{SiO}_4$  stretching and at 483  $\text{cm}^{-1}$  for modes of octahedral  $\text{MgO}_6$ . In addition, the broad band centered at 3400  $\text{cm}^{-1}$  ascribed to O–H band. It is also worth to note that our obtained results were similar to the previous studies [50, 51].

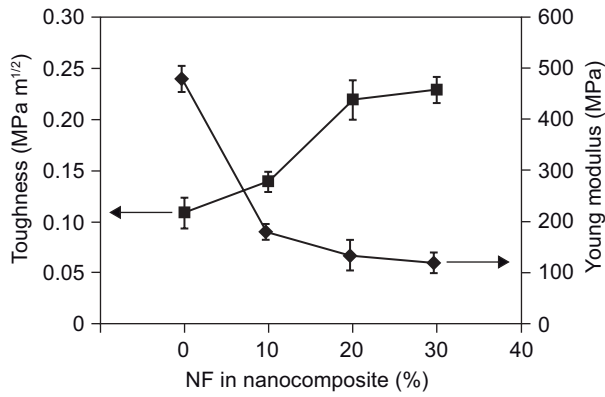
#### Mechanical properties

As NF ceramic shows a significant improvement in the fracture toughness, it can be used as an alternative for enhancing the toughness. Since the fracture toughness of different materials can be modified by adjusting the NF content, the influence of NF content on the fracture toughness of the prepared samples was investigated. The Elastic modulus and fracture toughness of the samples are shown in Figure 4a. The obtained results shows that the fracture toughness of the nanocomposites increased by further addition of NF from 10 to 30 wt. %. An acceptable fracture toughness of 0.22  $\text{MPa}\cdot\text{m}^{1/2}$  was obtained for the NC3 sample, whereas the Elastic modulus decreased with increasing the NF content. The Elastic modulus of the nanocomposites was strongly influenced by the NF content and decreased with increasing the NF content. To show the efficiency of NF addition on the toughness of the samples, the experimental model was modeled in ABAQUS software. The material properties were the same as experimental models and they were under compression load. Figure 4b to e) shows the final result in the software for all the samples (stress distribution versus normalized length). As expected, by further addition of NF to the glass matrix, the stress decreased. On other hand, NF powders can resist against compression force and it fractures later.

Toughness can be determined by measuring the area underneath the stress-strain curve, which is the energy of mechanical deformation per unit volume prior to fracture. Here, the results are based on normalized length, because they have similar length and we can compare

the data for every model. By calculating the area under the curves, it can be seen that the area increased by further addition of NF powder, and as a result the fracture toughness increased. The theoretical reason for toughness enhancement is that the composite materials act as polymer matrixes which are usually in plastic area. When a material is in plastic area, the molecular

separation is difficult and fracture has delay. Also, the added materials into the glass matrix are isotropic or distributed uniformly, which means that the material property, such as toughness, is independent of the position of nanocrystals within the materials. The discontinuous nature of nanocomposites can cause growing of cracks in all directions (not only in an exact direction). These two reasons can be physics reasons for increasing the fracture toughness by addition of NF powder.



### Sample characterization after *in vitro* assays in SBF

The essential condition for biomaterials to bond with living bone is the formation of a surface apatite layer in the body environment [52-56]. To determine the bioactivity of these materials, the prepared nanocomposite samples were subjected to *in vitro* testing using SBF solution. The samples were immersed in SBF at 37°C for 14 days. Morphological and textural properties of the biomaterials also indicate that soaking in SBF led to the formation of a layer near to the apatite on the surface of the samples.

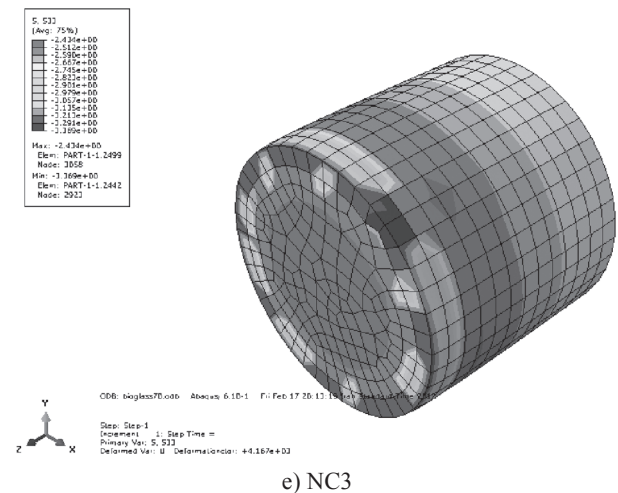
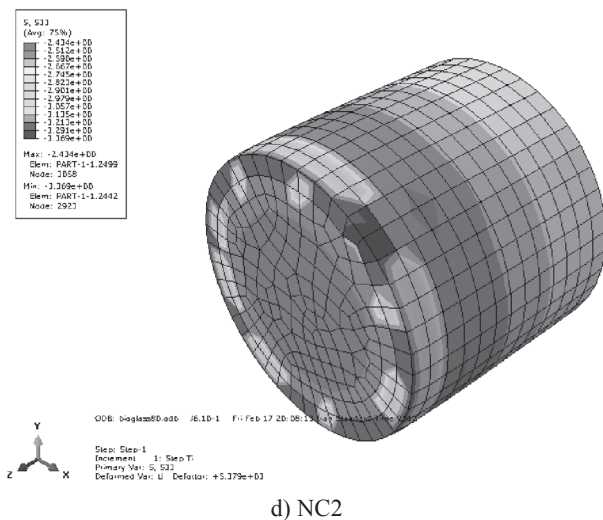
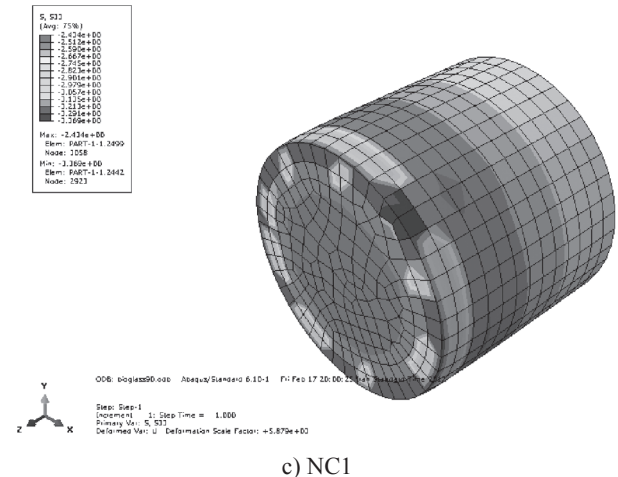
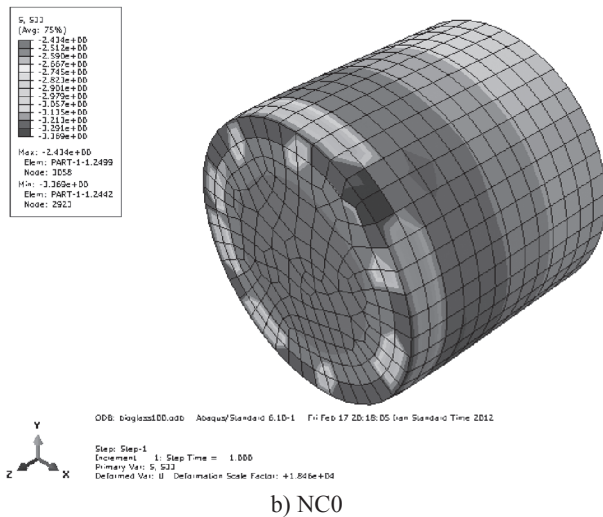


Figure 4. The elastic modulus and fracture toughness of the synthesized nanocomposite samples (a), stress distribution for b) NC0, c) NC1, d) NC2 and e) NC3 models in ABAQUS software, respectively.

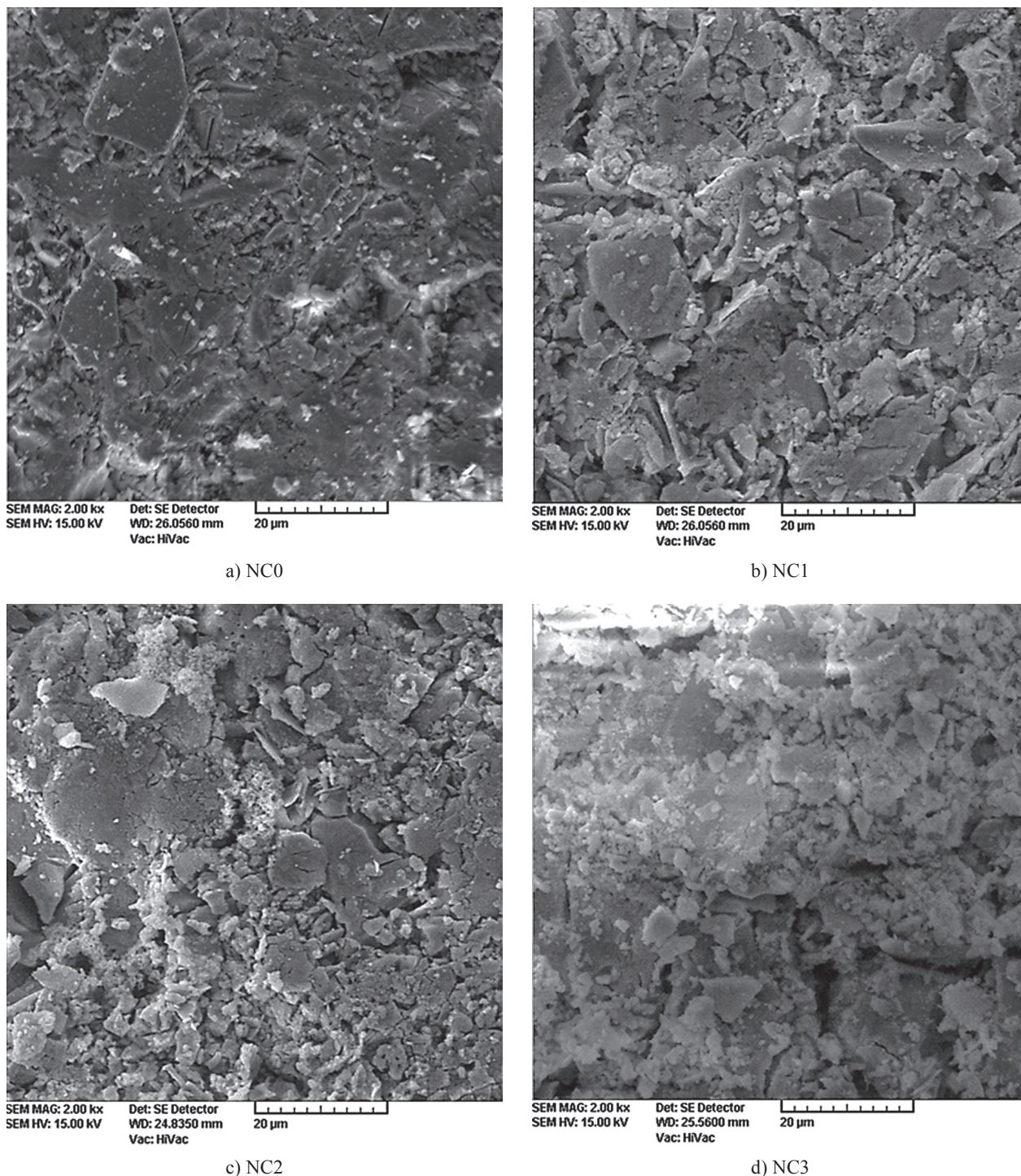


Figure 5. The SEM micrographs of the nanocomposite samples before immersion in SBF solution, a) NC0, b) NC1, c) NC2 and d) NC3.

Herein, apatite was incorporated into the surface of the nanocomposites *in situ* via the SBF technique. Figure 5 and 6 show SEM micrographs of the nanocomposite samples before and after immersion for 14 days, respectively. According to the observations, scattered and small particles were covered on the surface of the nanocomposites after 14 days of immersion which is clearly shown in Figure 6. The whole wall surfaces of

the nanocomposites were covered by a layer of apatite, and the underlying surfaces were not clearly observable and in all of the samples there can be seen the apatite particles which formed on the surfaces after soaking in SBF. According to the observations, addition of NF particles to the BG phase did not significantly change its bioactivity, and the prepared nanocomposites are still highly bioactive [57].

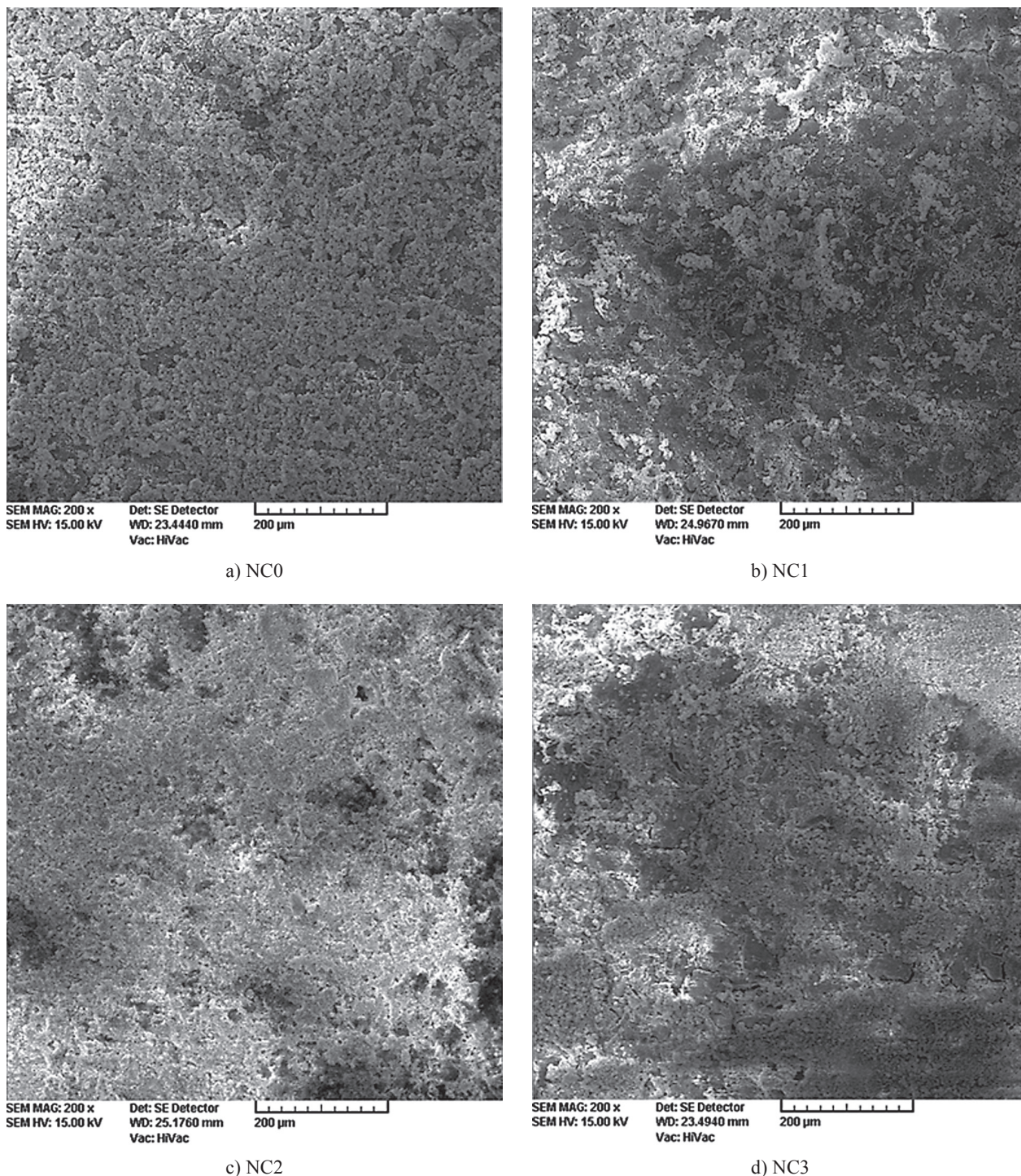


Figure 6. The SEM micrographs of the nanocomposite samples after immersion in SBF solution, a) NC0, b) NC1, c) NC2 and d) NC3.

After 14 days, all samples were completely covered with a newly formed layer. The apparition of Ca–P formations after immersion in SBF was established by EDX analysis. After 14 days, EDX analyses showed an increase in Ca and P and a decrease in Si (the data not presented). There was also a development in the molar Ca/P ratio which corresponded to non-stoichiometric biological apatite. For the sample NC3, the molar Ca/P ratio ranged from 1.33 (non-stoichiometric HCA) to 1.67,

and the whole surface of the sample was covered with Ca–P particles which created a dune-like apatite layer. The results demonstrated the gradual development of apatite on the surface of the sample containing higher amount of BG. This behavior of this kind of BG material was previously described by Mozafari et al. [10]. Figure 6 shows that the Ca/P ratios of different samples after immersion in SBF.

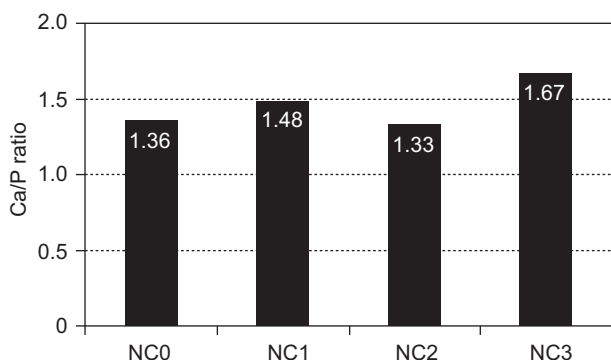


Figure 7. The Ca/P ratios of different samples after soaking in SBF.

### CONCLUSION

In conclusion, the experiments provide data to support the use of the nanocomposites in bone repair applications. Biomineralization studies showed that the deposition apatite phase on the surface of the nanocomposites ascertaining the bioactive nature of them. Here, it is obvious that the applying BG/NF nanocomposites are notable from different points of view including highly bioactivity and higher toughness quality of with increasing the amount of NF nanoparticles.

### References

- Niihara K.: *J. Ceram. Soc. Jpn.* 99, 945 (1991).
- Kuntz J.D., Zhan G.D., Mukherjee A.K.: *MRS Bull.* 29, 22 (2004).
- Harmer M.P., Chan H.M., Miller G.A.: *J. Am. Ceram. Soc.* 75, 1715 (1992).
- Hench L.L.: *Curr. Orthop.* 14, 7 (2000).
- Hench L.L., West J.K.: *Life Chem. Rep.* 13, 187 (1996).
- Hench L.L. in: *Handbook of bioactive ceramics*, p. 7, ed. Yamamuro T., Hench L.L., Wilson J., CRC Press, Boca raton, 1990.
- Ylanen H., Karlsson K.H., Itala A., Aro H.T.: *J. Non-Cryst. Solids* 275, 107 (2000).
- Hench L.L., LaTorre G.P. in: *Bioceramics*, p. 67–74, ed. Yamamuro, Kokubo, Nakamura, Kobunshi Kankokai Press 1993.
- Saravanapavan P., Jones J.R., Pryce R.S., Hench L.L.: *J. Biomed. Mater. Res.* 66A, 110 (2003).
- Mozafari M., Moztarzadeh F.: *J. Non-Cryst. Solids* 356, 1470 (2010).
- Mozafari M., Moztarzadeh F., Rabiee M., Azami M., Moztarzadeh Z.: *Adv. Compos. Lett.* 19, 91 (2010).
- Mozafari M., Moztarzadeh F., Rabiee M., Azami M., Moztarzadeh Z., Nezafati N.: *Ceram. Inter.* 36, 2431 (2010).
- Mozafari M., Rabiee M., Azami M., Maleknia S.: *Appl. Surf. Sci.* 257, 1740 (2010).
- Hamlekhan A., Mozafari M., Nezafati N., Azami M., Hadipour H.: *Adv. Compos. Lett.* 19, 123 (2010).

- Vallet R.M., Victoria R.C., Salinas J.A.: *Eur. J. Inorg. Chem.* 6, 1029 (2003).
- Radin S., Ducheyne P., Rothman B., Conti A.: *J. Biomed. Mater. Res.* 37, 363 (1997).
- Nezafati N., Moztarzadeh F., Hesaraki S., Mozafari M., Samadikuchaksaraei A., Hajibaki L., Gholipour M.: *Key Engineering Materials* 493-494, 74 (2012).
- Mardare C.C., Mardare A.I., Fernandes J.R.F., Correia R.N.: *J. Eur. Ceram. Soc.* 23, 1027 (2003).
- Kim S.R., Lee J.H., Kim Y.T., Riu D.H., Jung S.J., Lee Y.J., Chung S.C., Kim Y.H.: *Biomaterials* 24, 1389 (2003).
- Webster T.J., Massa-Schlueter E.A., Smith J.L., Slamovich E.B.: *Biomaterials* 25, 2111 (2004).
- Wu C.T., Chang J.: *Mater. Lett.* 58, 2415 (2004).
- Fathi M.H., Kharaziha M.: *Mater. Lett.* 62, 4306 (2008).
- Ni S., Chou L., Chang J.: *Ceram. Int.* 33, 83 (2007).
- Ni S., Chou L., Chang J.: *J. Mater. Sci.: Mater. Med.* 19, 359 (2008).
- Mitchell M.B.D., Jackson D., James P.F.: *J. Sol-Gel Sci. Technol.* 15, 211 (1999).
- Mitchell M.B.D., James P.F., Jackson D.: *J. Sol-Gel Sci. Technol.* 13, 359 (1998).
- Mitchell M.B.D., Jackson D., James P.F.: *J. Non-Cryst. Solids* 225, 125 (1998).
- Cottom B.A., Mayo M.J.: *Scripta Mat.* 34, 814 (1996).
- Cullity B.D.: *Elements of Xray Diffraction*, Prentice Hall, Addison Wesley, 1978.
- Edelstein A.S., Cammarata R.C.: *Nanomaterials: Synthesis, Properties and Applications*. Institute of Physics (IOP), England 1996.
- Fathi M.H., Kharaziha M.: *Mater. Lett.* 63, 1458 (2009).
- Ghosh A., Suri A.K., Rao B.T., Ramamohan T.R.: *J. Am. Ceram. Soc.* 90, 2015 (2007).
- Du C., Cui F.Z., Zhu X.D., Groot Kde.: *J. Biomed. Mater. Res.* 44, 407 (1999).
- Gutwein L.G., Webster T.J.: *J. Nanoparticle Res.* 4, 231 (2002).
- Kharaziha M., Fathi M.H.: *Ceram. Int.* 35, 2449 (2009).
- Pokrovsky O.S., Schott J.: *Geochimica et Cosmochimica Acta* 64, 3313 (2000).
- Saberi A., Alinejad B., Negahdari Z., Kazemi F., Almasi A.: *Mater. Res. Bull.* 42, 666 (2007).
- Kokubo T., Takadama H.: *Biomaterials* 27, 2907 (2006).
- Cai H., Shoelson B., Chadwick R.S.: *Proc. Natl. Acad. Sci. USA* 101, 6243 (2004).
- Iwasa K.H., Adachi M.: *Biophys. J.* 73, 546 (1997).
- Ravarian R., Moztarzadeh F., Solati Hashjin M., Rabiee S.M., Khoshakhlagh P.: *Ceram. Inter.* 36, 291 (2010).
- Salinas A.J., Martin A.I., Vallet-Regi M.: *J. Biomed. Mater. Res.* 61, 524 (2002).
- De Aza P.N., Fernandez-Pradas J.M., Serra P.: *Biomaterials* 25, 1983 (2004).
- Sarmiento C., Luklinska Z.B., Brown L., Anseau M., De Aza P.N., De Aza S., Hughes F.J., McKay I.J.: *J. Biomed. Mater. Res.* 69A, 351 (2004).
- De Aza P.N., Luklinska Z.B., Martinez, Anseau M.R., Guitian F., De Aza S.: *J. Microsc.* 197, 60 (2000).
- De Aza P.N., Luklinska Z.B., Anseau M.R., Guitian F., De Aza S.: *J. Dent.* 27, 107 (1999).

47. Fernández-Pradas J.M., Serra P., Morenza J.L., De Aza P.N.: *Biomaterials* 23, 2057 (2002).
  48. Yang H., Prewitt C.T.: *Am. Mineral.* 84, 929 (1999).
  49. Lambers J., Hess P.: *J. Appl. Phys.* 94, 2937 (2003).
  50. Duffy T.S., Zha C.S., Downs R.T., Mao H.K., Hemley R.J.: *Nature* 378, 170 (1995).
  51. Libowitzky E., Beran A.: *Phys. Chem. Minerals* 22, 387 (1999).
  52. Nezafati N., Moztarzadeh F., Mozafari M.: *Key Engineering Materials* 493-494, 209-214 (2012)
  53. Hamlekhhan A., Mozafari M., Nezafati N., Azami M., Samadikuchaksaraei A.: *Key Engineering Materials* 493-494, 909-915 (2012).
  54. Azami M., Jalilifiroozinezhad S., Mozafari M.: *Key Engineering Materials* 493-494, 626-631 (2012).
  55. Mozafari M., Moztarzadeh F. in: 1<sup>st</sup> Middle East Conference on Biomedical Engineering (IEEE), Sharjah, UAE 2011.
  56. Hamlekhhan A., Mozafari M., Nezafati N., Azami M., Hadipour H.: *Advanced Composites Letters* 19, 123 (2010).
  57. Yazdanpanah A., Kamalian R., Moztarzadeh F., Ravarian R., Mozafari M., Tayebi L., *Ceramics International* 38, 5007 (2012).
-